Nano Energy (2015) 13, 491–499

Available online at www.sciencedirect.com

ScienceDirect

journal homepage: www.elsevier.com/locate/nanoenergy

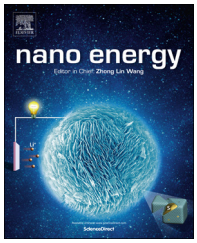

RAPID COMMUNICATION

Synergistic photocurrent addition in hybrid quantum dot: Bulk heterojunction solar cells

Gi-Hwan Kim[a,b], Bright Walker[a], David Zhitomirsky[b], Jungwoo Heo[c], Seo-Jin Ko[a], Jongnam Park[a], Edward H. Sargent[b,*], Jin Young Kim[a,**]

[a]School of Energy and Chemical Engineering, Ulsan National Institute of Science and Technology (UNIST), Ulsan 689-798, South Korea
[b]Electrical and Computer Engineering, University of Toronto, 10 King's College Road, Toronto, ON, Canada M5S 3G4
[c]Department of Physics, Ulsan National Institute of Science and Technology (UNIST), Ulsan 689-798, South Korea

Received 26 November 2014; received in revised form 14 February 2015; accepted 15 March 2015
Available online 24 March 2015

KEYWORDS
Hybrid solar cells;
Organic;
Quantum dot;
Quantum dot solar cells;
Bulk-heterojunction solar cells

Abstract
We investigate the effect of a thin PbS quantum dot (QD) layer on the performance of hybrid quantum-dot-organic solar cells (QD-OSCs). The PbS QD layer is able to function as a photosensitizing layer to improve short circuit current density (J_{SC}) and power conversion efficiency (PCE) by exploiting solar flux in the near infrared region up to 1100 nm. The increase in J_{SC} is well represented by changes observed in the external quantum efficiency of devices with and without the PbS QD layer, including the region of the first exciton transition where only the PbS QD layer absorbs. Remarkably, enhanced performance was observed in QD-OSCs consisting of just a 13 nm thick PbS QD layer and 150 nm PTB7:$PC_{71}BM$ layer, exhibiting a J_{SC} of 17.0 mA cm^{-2}, and PCE of 8.30% (8.58% for champion device) compared to reference devices without PbS QD which produced a J_{SC} of 15.4 mA cm^{-2} and PCE of 7.56%.

Introduction

In recent years, the field of solar cells has witnessed rapid growth with the development of a range of new materials and device architectures. Over 10% power conversion efficiency (PCE) has been reported using organic materials

*Corresponding author. Tel.: +1 416 946 5051; fax: +1 416 971 3020.
**Corresponding author. Tel.: +82 52 217 2911; fax: +82 52 217 2909.
E-mail addresses: ted.sargent@utoronto.ca (E.H. Sargent), jykim@unist.ac.kr (J. Young Kim).

http://dx.doi.org/10.1016/j.nanoen.2015.03.025
2211-2855/

[1-4] while 8% PCE has been reported with quantum dot (QD) materials [5-8]. The best organic and QD materials however, still result in much lower PCEs than inorganic solar cells such as Si, GaAs, CdTe or Cu(In,Ga)Se_2 [9]. Nonetheless, these new technologies garner much commercial and academic interest due to their strengths such as flexible substrate compatability, low cost, and facile solution fabrication which make them appealing for next generation solar cells. Extensive research has focused on the use of lead chalcogenide nanocrystals (PbS and PbSe) because of their desirable properties including facile synthesis from earth-abundant elements, easily and widely tunable band gaps and light absorption throughout the visible regions to the near-infrared (NIR) affording the potential for large photocurrents compared to other organic and inorganic materials [10,11]. Moreover, the possibility of exploiting multiple exciton generation raises the theoretical limit of PCE to as high as 64% [12-14]; something inaccessible with conventional bulk semiconductor photovoltaic materials.

Several groups have investigated using a combination of PbS QDs and a conjugated polymer network to prepare hybrid devices, with the aim of extending the absorption range of the resultant photovoltaic devices further into the near infrared. Such approaches may incorporate the QDs directly into the polymer matrix [15,16], thus requiring that the photogenerated electron–hole pair is separated and each carrier is injected into its corresponding transport phase. Despite promising results, these hybrid devices have yet to yield higher PCEs than pure-phase QD devices. This is likely due to the ease with which photo-generated electrons and holes recombine at the conjugated polymer/QD interface, and also to the shortcomings of the QD phase as a majority carrier transport material. This has prompted investigations of charge and energy transfer mechanisms between QD and organic materials such as conjugated polymers and fullerene derivatives [17,18]. Solution processing of polymer:PbS QD blends poses additional challenges due to the need for ligand exchange in the PbS QDs and degradation of polymer BHJs when exposed to solvents and ligands used during ligand exchange. Given the disadvantages and poor performance observed to date in mixed polymer:PbS QD active layers, an improved approach would leverage a bulk heterojunction (BHJ) comprised of a polymer:fullerene blend interfaced with a separate PbS QD layer, rather than intermixing of the QD and polymer phases. This approach could preserve the optimal materials properties of each phase and enable their efficient combination into a hybrid device. The utility of this approach was first demonstrated by Luther and coworkers, [19] who employed a thick *p*-type PbS QD layer and a thin PSBTBT:PCBM BHJ thus modifying the interface at the Schottky junction between the PbS layer and the low work function metal. A respectable improvement in short circuit current density (J_{SC}) was achieved compared to either the polymer BHJ or the QD device alone, however, the open circuit voltage (V_{OC}) degraded significantly with respect to the pure-phase BHJ counterpart and was somewhat lower than the phase-pure QD device as well.

In this report, we have studied the effects of PbS thickness on carrier diffusion and used this knowledge to demonstrate hybrid QD-organic solar cells (QD-OSCs) which do not suffer losses in V_{OC} or fill factor (FF) due to incorporation of the PbS layer. By utilizing a PbS QD layer as a thin photosensitizing layer (PSL), we are able achieve a high *J*sc and PCE by exploiting solar flux in the NIR region up to 1100 nm. The thickness of the QD film is judiciously chosen to coincide with its minority carrier (electron) diffusion length, and as a result, photo-generated electrons in the PbS QD layer are efficiently transported to the lowest unoccupied molecular orbital band of $PC_{71}BM$ without recombining. This careful tailoring of the PbS QD layers within the BHJ solar cells allows them to perform efficiently as PSLs without adversely affecting other device parameters.

We took the view that, in principle, the combination of the PbS QD and BHJ layers should yield improved device performance, but that the criteria that would need to be met to leverage these materials in tandem required deeper insight, modeling, and improved device designs. Although it is expected that light absorbed in the PbS QD layer will contribute to the photocurrent and J_{SC} produced by the device, the impact on other device parameters is unclear. Thus, a detailed mechanistic understanding of charge generation and extraction is required for the PbS QD layer.

Experimental section

Device fabrication

QD-OSCs devices were fabricated using the following procedure: Clevios PH PEDOT:PSS purchased from H. C. Starck (Germany) was spin-coated on ITO coated glass substrates at 5000 rpm for 60 s and then baked at 140 °C for 10 min. PbS layers were then deposited by spin-coating a 10, 30, and 50 mg ml^{-1} solution of QDs in octane at 2500 rpm for 10 s in air. The oleate ligands of the QDs were exchanged by spin-coating a 1% (v/v) 3-mercaptopropionic acid (MPA) in methanol solution at 2500 rpm for 10 s, then sequentially rinsing with methanol and octane at 2500 rpm for 10 s in an adaptation of a previously reported procedure [20]. PbS QDs were spin-coated only one time in this way to achieve PbS QD films of variable thickness (6, 13, and 30 nm). Next, a chlorobenzene solution consisting of PTB7 (1 wt%), $PC_{71}BM$ (1.5 wt%), and 1,8-diiodooctane (3 vol%) was spin-cast at 1000 rpm on top of the PbS QD layer in nitrogen filled glovebox. Finally, samples were transferred to a vacuum chamber ($<10^{-6}$ Torr), and a 100 nm thick Al electrode was thermally evaporated on top of the BHJ layer through a shadow mask. The deposited Al electrode area defined the active area of the devices as 13 mm^2.

For the device ITO/PEDOT:PSS/PbS QD/ZnO/Al, the ZnO layer was deposited by diluting a diethylzinc solution (Aldrich, 15 wt% in toluene) with two parts tetrahydrofuran (note: the un-diluted diethyl zinc solution is highly reactive towards air and should be handled inside a glovebox; after dilution with THF, the solution becomes less reactive, however, appropriate safety precautions should be taken in case of an accidental spill or fire), filtering through a 0.45 μm PTFE syringe filter and spin coating at 3000 rpm for 30 s in air. The ZnO precursor solution was kept closed in a 4 mL vial while not in use and spin-coated by rapidly dispensing 25 μL onto an already spinning substrate using a micropipette with a plastic tip. The precursor solution forms solid ZnO on the pipette tip over time when exposed to air,

therefore, a new plastic tip was used for each substrate to avoid the formation of large ZnO particulates. The ZnO layer was then annealed in air on a hot plate at 110 °C for 10 min, yielding a ZnO layer with a thickness of 60 nm.

Film characterization

UV-vis-NIR absorption spectra were measured on a Varian Cary 5000 spectrophotometer. The cross-sectional image of the device was measured using a JEM-2100F (Cs corrector) HR-TEM. External quantum efficiency (EQE) measurements were obtained by using a PV measurements OE system equipped with a Xenon arc lamp where monochromated light was chopped at a frequency of 100 Hz and photocurrent response detected with a lock-in amplifier and compared to a reference silicon photodiode. Photovoltaic device characteristics were measured inside a glove box using a high quality optical fiber to guide light from a xenon arc lamp. Current density–voltage (*J-V*) characteristics of the devices were measured using a Keithley 2635A Source Measure unit. Light intensity was calibrated using an NREL certified standard silicon solar cell with a protective window containing KG5 filter glass. AFM measurements were performed using a Multimode V from Veeco (USA) in a tapping mode using silicon tips with a resonant frequency of ~300 kHz.

Optical modeling

Optical modeling was performed via transfer matrix modeling based on Fresnel's equations for stacks of materials with different optical constants (**n**, **κ**). Optical constants of ITO, PEDOT:PSS and PbS QD layers were obtained as previously reported [20]. Reflectance data for Al and Au were taken from the literature [21,22]. **κ** values were calculated from the absorption coefficient (α) using the relationship $\boldsymbol{\kappa}=\lambda\alpha/4\pi$. **n** values were taken from *k* values using the Kramers-Kronig relationships assuming an average value of 2 for the range of wavelengths from 400 to 1100 nm. The (α) values of PTB7:$PC_{71}BM$ films were taken as the average value calculated from absorption measurements of films with four different thicknesses in which the thickness was measured nine times for each sample using an atomic force microscope. The thickness' of PTB7:$PC_{71}BM$ layers for optimized devices were measured by atomic force microscopy and found to be ~90 nm for devices without the PbS layer and ~150 nm for devices with the PbS layer [23].

Electronic modeling

Hybrid devices were simulated with SCAPS [24,25] simulation software. The parameter space is available in Table S1 in the Supporting information [26]. AM1.5 excitation spectrum and experimental absorption data were used to obtain the generation rate. The bandgaps chosen represent the effective bandgap of the polymer BHJ (highest occupied molecular orbital of donor and lowest unoccupied molecular orbital of acceptor) and the first excitonic transition of the PbS. The band alignment was chosen equal to avoid effects of band bending that could introduce electric fields resulting in drift.

Results and discussion

Our proposed architecture is based on a BHJ comprised of PTB7:$PC_{71}BM$ and a *p*-type PbS QD layer, with the full device stack shown in Figure 1 Upon absorption of a photon (Figure 1a), the PbS QD layer generates electron-hole pairs that split as the holes migrate towards the anode through the PEDOT:PSS layer, while the electrons are transferred to the electron transporting $PC_{71}BM$ in the BHJ layer before finally reaching the cathode. Because the Fermi energies of PEDOT:PSS and the PbS QD layer are similar (both near 5.0 eV), the PEDOT:PSS should not contribute significantly to the depletion of the PbS QD layer. Similarly, the low intrinsic carrier density of the BHJ layer is unlikely to cause significant depletion in the PbS QD layer, thus, any carriers passing through the PbS QD layer must rely on diffusion to be extracted. Holes, being the majority carriers, are able to diffuse more efficiently with a low rate of recombination. Hence, minority electrons generated in the PbS QD layer must have sufficient diffusion length to reach the PbS QD/BHJ junction in hopes of contributing to the device current, otherwise they may recombine (Figure 1b), potentially also degrading other device parameters. The PTB7:$PC_{71}BM$ phase generates photocurrent via photo-induced electron transfer from PTB7 to the $PC_{71}BM$. It should be noted that electron transfer from PTB7 to the PbS QD layer is also energetically favorable and this process may occur in the present architecture; however, it is not observed to represent a significant loss mechanism. Because there is $PC_{71}BM$ in direct contact with the PbS QD layer, such electrons are expected to subsequently back-transfer to the $PC_{71}BM$ in the BHJ phase. The presence of an electron-blocking PEDOT:PSS layer ensures that they do not diffuse to the anode, and subsequently follow a path through the BHJ phase towards the cathode.

Drawing inspiration from recently reported works on transport in QD materials [27,28], we designed self-consistent optoelectronic simulations (Table S1) based on a BHJ comprised of PTB7:$PC_{71}BM$ and a *p*-type PbS QD layer, with the full device stack shown in Figure 1. By tuning both diffusion length and thickness in the *p*-type PbS QD layer, we demonstrate the critical importance of diffusion length in order to achieve improved device performance (Figure 1c). For the *p*-type PbS QD materials employed in this study, diffusion lengths are limited to <30 nm [27], thus mandating thin QD active layers for improved performance. These optoelectronic simulations also reveal (Figure S1, Figure 1c) that increasing the PbS QD layer thickness will result in pronounced degradation to the V_{OC} and FF unless diffusion lengths are sufficiently high, while the J_{SC} will continue to increase. Thus, tailoring the PbS QD layer will mandate improving the J_{SC} with the careful choice of thickness to avoid degradation in other device parameters in light of the minority carrier diffusion lengths in these materials.

QD-OSCs were fabricated in the following device structure: ITO/PEDOT:PSS/PbS QD/PTB7:$PC_{71}BM$/Al. Figure 2a shows UV-vis absorption spectra of spin-cast films including the PTB7:$PC_{71}BM$ BHJ, PbS, and PbS QD/BHJ bilayer. The BHJ films absorb throughout the visible region up to 770 nm wavelength, while the PbS QD layer absorbs photons in the NIR region up to 1100 nm, with a clear first excitonic transition peak at ~1000 nm. When the BHJ layer is deposited on top of the PbS QD layer, the absorption

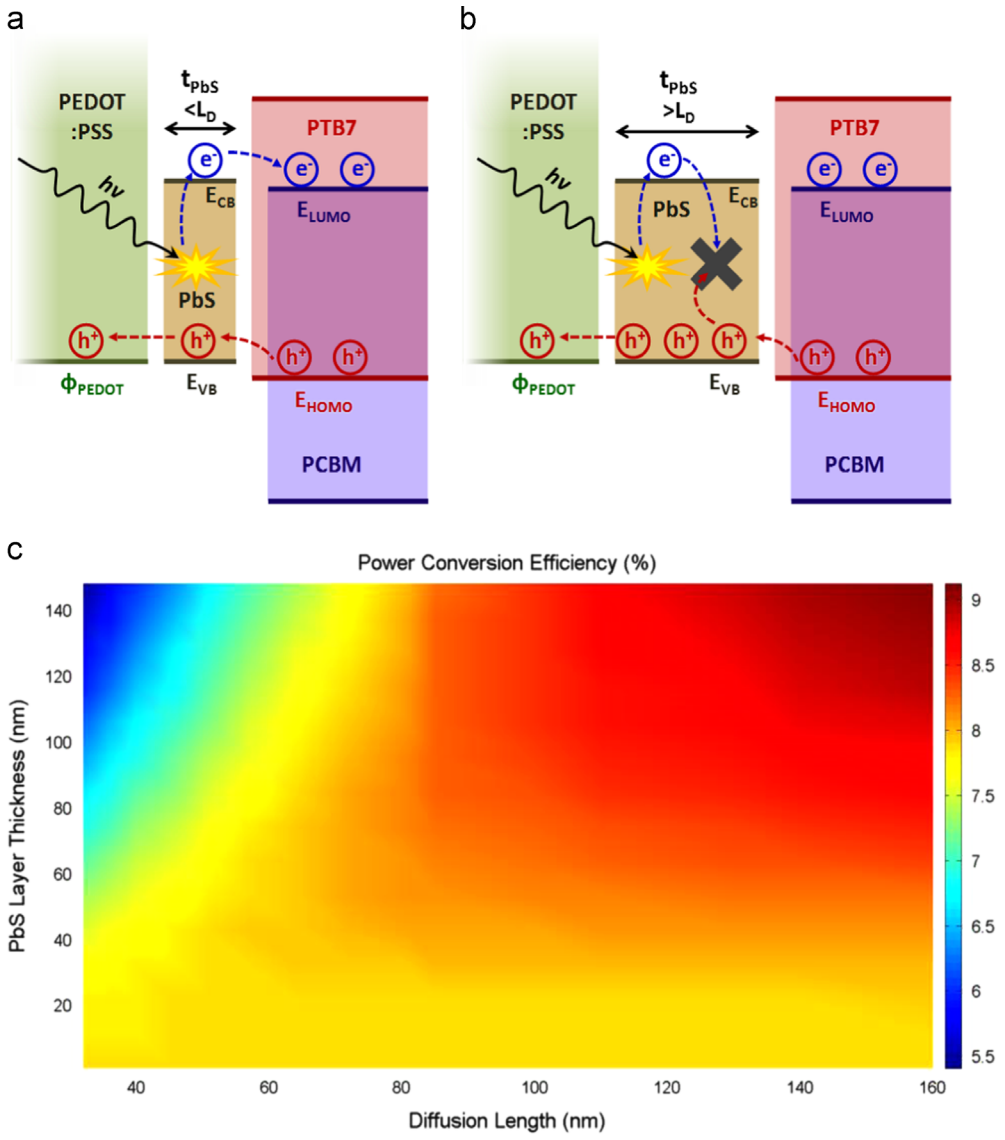

Figure 1 Proposed device architecture for the incorporation of a *p*-type PbS layer with a PTB7:PCBM BHJ. (a) e-h pair generation and successful extraction through the materials stack by carriers migrating to their transport phases. (b) A thicker PbS QD layer with insufficient diffuion length go guarantee carrier extraction, thus resulting in charge recombination. (c) Self-consistent optoelectronic simulations revealing the importance of diffusion length and thickness for improved device performance in these hybrid devices.

spectrum exhibits features consistent with the sum of the absorbance of the BHJ layer and PbS QD layer together with optical interference between the layers. The enhanced absorbance of the hybrid PbS QD/BHJ structure results in additional photocurrent generation, with improved device performance. Absorption spectra of PbS QD films with various thickness (6 nm, 13 nm, and 30 nm) as well as PbS QD/BHJ bilayers on glass substrates are shown in Figure S2. Although the PbS QD layers are fairly thin, the optical absorbance changes dramatically, resulting in optical interference caused by high refractive index of the PbS QD layer [20] that depend on the thickness of the PbS QD layer. A detailed energy band diagram of the QD-OSCs, ITO/PEDOT:PSS/PbS QD/PTB7:$PC_{71}BM$/Al, is shown in Figure 2b.

Figure 3a depicts the device architecture. Figure 3b shows cross-sectional high resolution transmission electron microscope (HR-TEM) images of an optimized QD-OSCs device. Individual layers corresponding to PEDOT:PSS, PbS QD, and BHJ layers with thicknesses of 40 nm, 13 nm and 150 nm, respectively, can be clearly distinguished. Additional HR-TEM images of the QD-OSCs architecture at various thickness of PbS QD can be found in Figure S3. A magnified image of the PbS QD layer reveals lattice fringes within individual PbS nanoparticles having diameters of 3–4 nm. The HR TEM image shows that the BHJ layer and PbS QD layer are well intermixed at the interface which facilitates rapid charge transfer between PbS QD and organic layers. Atomic force microscopy images of thin PbS QD films show a layered structure where discreet monolayers of PbS QDs can clearly be distinguished in thin (6 nm) films as shown in Figures S4 and S5. For 6 nm films, the film does not completely cover the substrate, which is

exposed through circular holes in the film and is apparent as regions of high phase contrast. Although the average thickness of the film is 6 nm, the film actually is 0, 1 or 2 layers thick in some places; the bottom layer has a thickness of 6.7 nm while additional layers have a thickness of 5.0 nm (Figure S5). The difference in thickness between the bottom layer and subsequent layers is consistent with close-packing of the roughly spherical PbS QDs layers; a second layer of close packed spheres has a thickness which is 81.6% of the first layer (see inset, Figure S5), close to the observed ratio of ~75%. The thickness' of the layers are somewhat larger than the diameter of the QDs as measured by TEM, however, this observation is consistent with the presence of an outer MPA layer around the PbS QDs, which is transparent in the TEM images but is measured by the AFM probe. Discreet layers become less obvious in the 13 nm film while the 30 nm film exhibits a fairly uniform, amorphous structure.

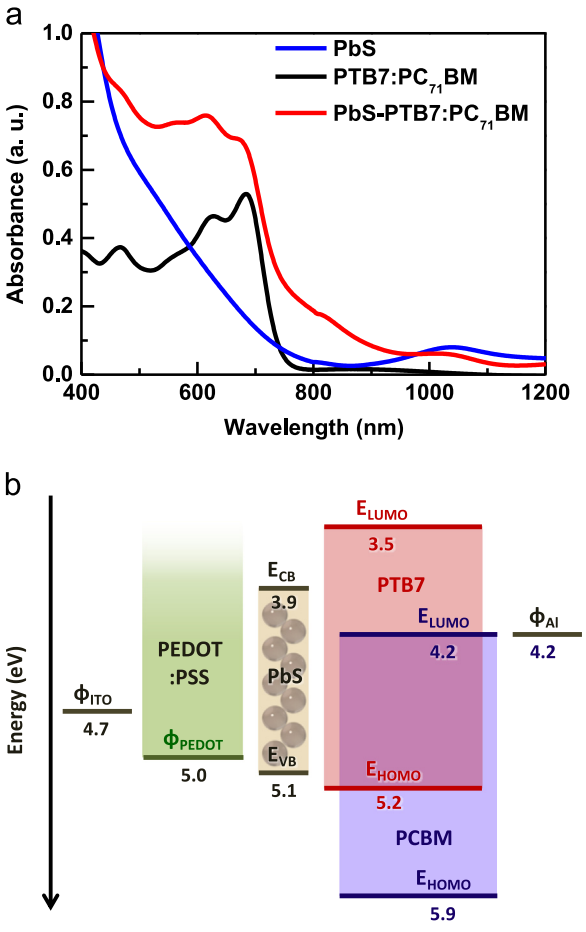

Figure 2 (a) Absorption spectra of films for BHJ, PbS QD, and PbS-BHJ (b) energy band diagram of QD-OSCs ITO/PEDOT:PSS/PbS QD/PTB7:$PC_{71}BM$/Al.

The *J-V* characteristics for photovoltaic devices prepared with the architecture ITO/PEDOT:PSS/PbS QD/BHJ/Al under 100 mW cm^{-2} AM1.5G irradiation are shown in Figures 4a and S6 with comparison to a control device (ITO/PEDOT:PSS/BHJ/Al) without the PbS QD layer. Device parameters are summarized in Tables 1 and S2. Optimized devices (with a PbS QD layer of 13 nm and BHJ layer of 150 nm thickness) exhibited a J_{SC} of 17.0 mA cm^{-2}, a V_{OC} of 0.74 V, FF of 0.66, R_S of 6.8 Ω cm^2, R_{sh} of 128 kΩ cm^2, and PCE of 8.30%. The reference BHJ device (90 nm BHJ thickness) without the PbS QD layer produced a J_{SC} of 15.4 mA cm^{-2}, V_{OC} of 0.74, FF of 66%, R_S of 8.2 Ω cm^2, R_{sh} of 68 kΩ cm^2, and PCE of 7.56%. The reference device characteristics are comparable to other reports of PTB7:$PC_{71}BM$ devices [4,29-31]. The effect of PbS QD layer thickness is investigated by changing the thickness from 6 nm to 240 nm with an optimized thickness of the BHJ as shown in Figure S6 and Table S2. The electrons must be extracted from the PbS QD layer into the electron transporting $PC_{71}BM$. They rely on diffusion to do so, which is known to be around 30 nm for such PbS QD layers, [27] hence the thickness of the PbS QD layer is limited to below this value. These trends are in agreement with the optoelectronic simulations presented in Figures 1c and S1, though agreement in absolute performance will require an increased understanding of the BHJ/PbS QD interface and material parameter changes upon processing required to combine the two layers. Evidently, past a certain thickness threshold all parameters are dramatically reduced due to recombination in the PbS QD layer and increased series resistance. Thus, we conclude that through the careful choice of a PbS QD layer thickness it is possible to contribute to photocurrent generation without significantly reducing other device parameters as long as the PbS QD layer thickness is tailored in accordance with the minority carrier diffusion length within this layer.

The increase in current density is well represented by changes observed in the external quantum efficiency (EQE) of devices with and without the PbS QD layer, as shown in Figure 4b. The QD-OSCs incorporating the PbS QD layer shows a significant increase in EQE in the spectral range of 400-600 nm, in addition to a new band of photocurrent

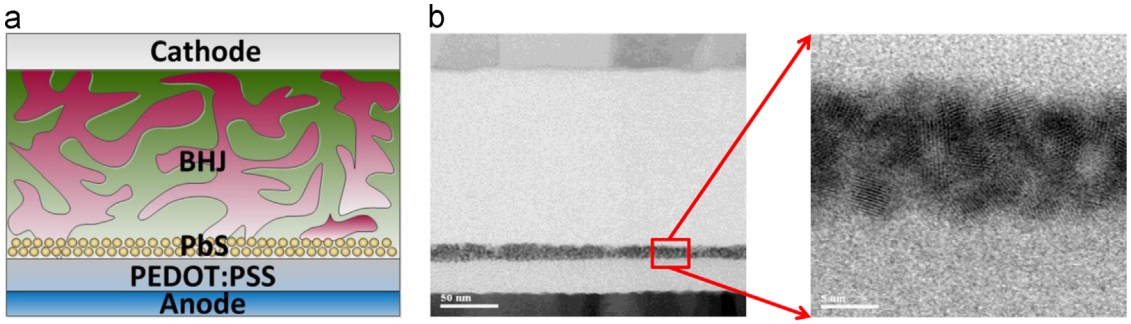

Figure 3 (a) Schematic device architecture of QD-OSCs (b) high resolution transmission electron microscope (HR-TEM) images of the QD-OSCs device with magnified PbS QD region between PEDOT:PSS and BHJ layers.

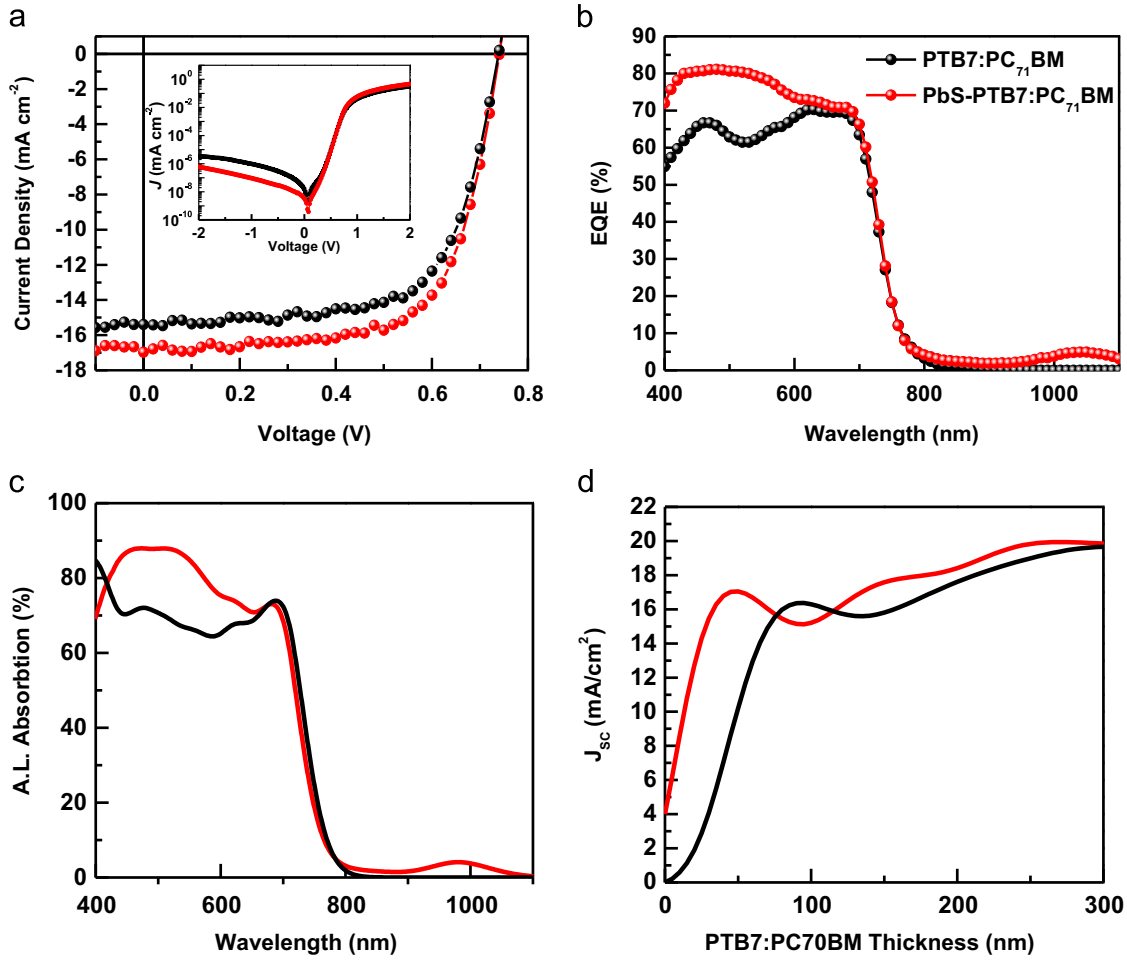

Figure 4 (a) *J-V* characteristics (b) external quantum efficiency of the optimized QD-OSCs with and without PbS QD layer (c) simulated active layer absorption with optimized thickness 150 nm for the BHJ layer, and 13 nm for the PbS QD layer (d) simulated short circuit current density in QD-OSCs as a function of PTB7:$PC_{71}BM$ layer thicknesses with optimized PbS thickness 13 nm obtained via transfer matrix modeling.

Table 1 Device characteristics of QD-OSCs with and without PbS QD layer.

Device configuration	PbS thickness [nm]	J_{SC} [mA cm^{-2}]	V_{OC} [V]	FF	η [%]	J_{SC} (Cal)[a] [mA cm^{-2}]
ITO/PEDOT:PSS/BHJ/Al	0	15.4	0.74	0.66	7.56	15.6
ITO/PEDOT:PSS/PbS QD/BHJ/Al	13	17.0	0.74	0.66	8.30	17.2

generation near 1000 nm corresponding to the first exciton transition of the PbS QD. These changes are consistent with the absorption spectrum of the PbS QD film. The highest EQE reached is 81.1% at 470 nm and a first excitonic transition peak shows a quantum efficiency of 4.9% at $\lambda = 1040$ nm. The EQE features closely match the absorption of PbS QD/BHJ as shown in Figure 2a.

For comparison, PbS QD/ZnO devices without the BHJ layer were also prepared. Interestingly, even a 13 nm layer of PbS QDs is able to generate a J_{SC} of 3.35 mA cm^{-2}, along with a V_{OC} of 0.53, FF of 41%, and PCE of 0.71% as shown in Figure S7 and Table S3. The QD-OSCs device shows a J_{SC} increase of 1.6 mA/cm^2 upon incorporating the PbS QD layer. Although this increase in J_{SC} is less than the PbS QD layer alone is able to generate (3.35 mA/cm^2), this is not unexpected for several reasons. The light absorbed by the PbS QD layer is unavailable to be absorbed by the PTB7 layer and the photocurrent produced by the PTB7:$PC_{71}BM$ layer decreases upon incorporation of the PbS QD layer. Additionally, the high refractive index of PbS QD may cause additional light to be reflected from the PEDOT/PbS QD layer interface compared to the PEDOT/PTB7:$PC_{71}BM$.

In order to quantify the effects of reflection and absorption in the PbS QD layer and further understand the optical phenomena occurring in the ITO/PEDOT:PSS/PbS QD/BHJ/Al structure, transfer matrix optical simulations were carried

out. The amount of light absorbed in the active layer (active layer absorption, ALA) was calculated using known or measured n and κ values for each material, taking into account the amount of light absorbed and reflected at each layer in the glass/ITO/PEDOT:PSS/PbS QD/BHJ/Al optical stack using a transfer matrix based on Fresnel's equations [32]. The calculated ALA spectrum of the BHJ layer in the glass/ITO/PEDOT:PSS/BHJ/Al architecture is compared to the spectrum of light absorbed by the BHJ and PbS QD layers in the glass/ITO/PEDOT:PSS/PbS QD/BHJ/Al architecture in Figure 4c, using the following (optimized) layer thicknesses: ITO - 150 nm, PEDOT:PSS - 40 nm, PbS QD - 13 nm, BHJ - 150 nm and Al - 100 nm. If the charge carrier extraction efficiency (or internal quantum efficiency (IQE)) is relatively constant for charge carriers generated by photons with different wavelengths of light, then the ALA spectrum should resemble the observed EQE (Figure 4b). The modeled ALA shows the same changes upon incorporation of the PbS QD layer that are observed in the EQE, including a broad increase in the range of 400–600 nm and a peak in the NIR at 1000 nm, corresponding to the first exciton transition of the PbS QD layer. These changes are consistent with light absorption by the PbS QD layer. From the amount of light absorbed in the active layer, the J_{SC} can be estimated assuming each absorbed photon leads to the generation and extraction of an electron–hole pair. Figure 4d shows a plot of the J_{SC} calculated in this manner for each device with and without PbS QD layer structures as a function of BHJ layer thickness. It should be noted that the first constructive interference maximum near 100 nm active layer thickness changes to a local minimum upon incorporation of the PbS QD layer, while the first destructive interference minimum changes to a constructive shoulder. This behavior is consistent with the observation that the optimal BHJ thickness is 150 nm when using the PbS QD layer. Calculated J_{SC}s of 15.8 mA cm^{-2} without PbS QD layer and 17.6 mA cm^{-2} with PbS QD layer are obtained in this manner. The optical simulation indicates that the PbS QD layer may contribute a photocurrent increase of 1.8 mA cm^{-2} in the QD-OSCs device, similar to the experimentally observed increase of 1.6 mA/cm^2.

To further investigate the effect of PbS QD on light absorption in the QD-OSCs, we carried out reflectance measurements in order to quantify the increase in absorption ($\Delta\alpha$, Eq. (1)) caused by the PbS QD layer [33].

$$\Delta\alpha(\omega) = -\left(\frac{1}{2}d\right) ln\left[\frac{I'_{out}(\omega)}{I_{out}(\omega)}\right] \quad (1)$$

here, d is the thickness of active layer, I_{out} is the intensity of the reflected light from the device without PbS QD layer, and I'_{out} is the intensity of the reflected light from the identical device with PbS QD layer. Figure 5a demonstrates that $\Delta\alpha(\omega) > 0$, that is, a clear increase in absorption is observed upon inserting the PbS QD layer. The calculated $\Delta\alpha(\omega)$ for the wavelength range 400–1100 nm is similar to the change in EQE (ΔEQE) upon incorporation of the PbS QD layer, as reported in Figure 5b. Some mismatch between $\Delta\alpha(\omega)$ and ΔEQE is expected, as $\Delta\alpha(\omega)$ is purely optical, whereas changes in EQE are influenced by charge carrier transport and recombination in addition to optical properties. This result indicates that the thin PbS QD layer (13 nm) causes a substantial increase in absorption in the device which is consistent with an increase in photocurrent generation as observed in the EQE.

Conclusions

The findings herein demonstrate the successful integration of a PbS QD layer with a polymer BHJ. The approach led for the first time to improved performance in state-of-the-art PTB7:$PC_{71}BM$ solar cells. This advance mandated that the mechanistic details of charge transport in the PbS QD layer be understood, something that was accomplished through optoelectronic simulations. Where previous approaches were unable to improve device performance with the integration of these two materials systems, our approach, guided by simulation, revealed the critical importance of the diffusion length in QD solids and the relationship with the QD layer thickness to yield optimal devices. Furthermore, optical simulations reveal added benefits in absorption due to refractive index difference in this materials

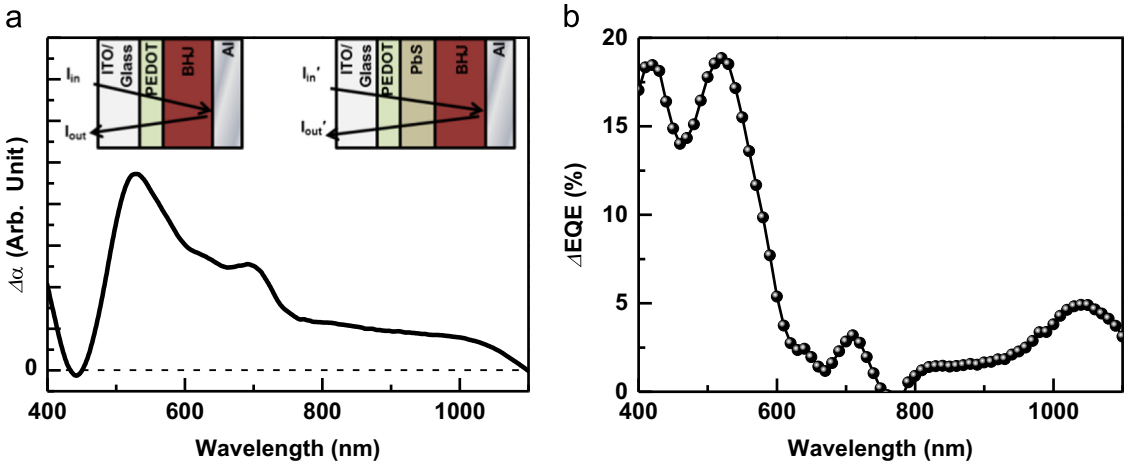

Figure 5 (a) Change in the absorption spectrum ($\Delta\alpha(\omega)$) due to the PbS layer architectures according to Eq. (1) and (b) comparison of the EQE enhancement (ΔEQE) with and without PbS QD layer on the structure ITO/PEDOT:PSS/PbS QD/PTB7:$PC_{71}BM$/Al.

stack. Our results pave the way for future improvement to hybrid QD/BHJ devices offering a robust framework for device optimization and high efficiency.

Acknowledgment

This research was supported by the BK21 Plus Program (META-Material-Based Energy Harvest and Storage Technologies, 10Z20130011057) funded by the Ministry of Education (MOE, Korea), the National Research Foundation of Korea Grant (NRF-2013R1A2A2A01015342), and the International Cooperation of the Korea Institute of Energy Technology Evaluation and Planning (KETEP) Grant funded by the Ministry of Knowledge Economy, South Korea (2012T100100740), D. Zhitomirsky would like to acknowledge support from the NSERC CGS D scholarship.

Appendix A. Supporting information

Supplementary data associated with this article can be found in the online version at http://dx.doi.org/10.1016/j.nanoen.2015.03.025.

References

[1] J.Y. Kim, K. Lee, N.E. Coates, D. Moses, T.-Q. Nguyen, M. Dante, A.J. Heeger, Science 317 (2007) 222.
[2] J. You, C.C. Chen, Z. Hong, K. Yoshimura, K. Ohya, R. Xu, S. Ye, J. Gao, G. Li, Y. Yang, Adv. Mater. 25 (2013) 3973.
[3] J. You, L. Dou, K. Yoshimura, T. Kato, K. Ohya, T. Moriarty, K. Emery, C.-C. Chen, J. Gao, G. Li, Nat. Commun. 4 (2013) 1446.
[4] H. Choi, J.-P. Lee, S.-J. Ko, J.-W. Jung, H. Park, S. Yoo, O. Park, J.-R. Jeong, S. Park, J.Y. Kim, Nano Lett. 13 (2013) 2204.
[5] J. Tang, K.W. Kemp, S. Hoogland, K.S. Jeong, H. Liu, L. Levina, M. Furukawa, X. Wang, R. Debnath, D. Cha, Nat. Mater. 10 (2011) 765.
[6] Z. Ning, Y. Ren, S. Hoogland, O. Voznyy, L. Levina, P. Stadler, X. Lan, D. Zhitomirsky, E.H. Sargent, Adv. Mater. 24 (2012) 6295.
[7] A.H. Ip, S.M. Thon, S. Hoogland, O. Voznyy, D. Zhitomirsky, R. Debnath, L. Levina, L.R. Rollny, G.H. Carey, A. Fischer, Nat. Nanotechnol. 7 (2012) 577.
[8] G.I. Koleilat, I.J. Kramer, C.T. Wong, S.M. Thon, A.J. Labelle, S. Hoogland, E.H. Sargent, Sci. Rep. 3 (2013) 2166.
[9] M.A. Green, K. Emery, Y. Hishikawa, W. Warta, E.D. Dunlop, Prog. Photovolt. 22 (2014) 1.
[10] I.J. Kramer, E.H. Sargent, Chem. Rev. 114 (2013) 863.
[11] J. Zhang, J. Gao, E.M. Miller, J.M. Luther, M.C. Beard, ACS Nano 8 (2013) 614.
[12] A. Nozik, Physica E 14 (2002) 115.
[13] R.J. Ellingson, M.C. Beard, J.C. Johnson, P. Yu, O.I. Micic, A.J. Nozik, A. Shabaev, A.L. Efros, Nano Lett. 5 (2005) 865.
[14] O.E. Semonin, J.M. Luther, S. Choi, H.-Y. Chen, J. Gao, A.J. Nozik, M.C. Beard, Science 334 (2011) 1530.
[15] J. Seo, S.J. Kim, W.J. Kim, R. Singh, M. Samoc, A.N. Cartwright, P.N. Prasad, Nanotechnology 20 (2009) 095202.
[16] Z. Liu, Y. Sun, J. Yuan, H. Wei, X. Huang, L. Han, W. Wang, H. Wang, W. Ma, Adv. Mater. 25 (2013) 5772.
[17] A.E. Colbert, E.M. Janke, S.T. Hsieh, S. Subramaniyan, C.W. Schlenker, S.A. Jenekhe, D.S. Ginger, J. Phys. Chem. Lett. 4 (2012) 280.
[18] E. Strein, A. Colbert, S. Subramaniyan, H. Nagaoka, C.W. Schlenker, E. Janke, S.A. Jenekhe, D.S. Ginger, Energy Environ. Sci. 6 (2013) 769.
[19] H.-Y. Chen, J. Hou, S. Dayal, L. huo, N. Kopidakis, M.C. Beard, J.M. Luther, Adv. Energy Mater. 1 (2011) 528.
[20] G.-H. Kim, B. Walker, H.-B. Kim, J.Y. Kim, E.H. Sargent, J. Park, J.Y. Kim, Adv. Mater. 20 (2014) 3321.
[21] D.Y. Smith, E. Shiles, M. Inokuti, in: Edward D. Palik (Ed.), Handbook of Optical Constants of Solids, Academic Press, Burlington, 1997, p. 369.
[22] D.W. Lynch, W.R. Hunter, in: Edward D. Palik (Ed.), Handbook of Optical Constants of Solids, Academic Press, Burlington, 1997, p. 275.
[23] H.R. Yeom, J. Heo, G.-H. Kim, S.-J. Ko, S. Song, Y. Jo, D.S. Kim, B. Walker, J.Y. Kim, Phys. Chem. Chem. Phys. 17 (2015) 2152.
[24] M. Burgelman, P. Nollet, S. Degrave, Thin Solid Films 361 (2000) 527.
[25] M. Burgelman, K. Decock, S. Khelifi, A. Abass, Thin Solid Films 535 (2013) 296.
[26] Z. Li, G. Lakhwani, N. Greenham, C. Mcneill, J. Appl. Phys. 114 (2013) 034502.
[27] D. Zhitomirsky, O. Voznyy, S. Hoogland, E.H. Sargent, ACS Nano 7 (2013) 5282.
[28] O. Voznyy, D. Zhitomirsky, P. Stadler, Z. Ning, S. Hoogland, E.H. Sargent, ACS Nano 6 (2012) 8448.
[29] H. Zhou, Y. Zhang, J. Seifter, S.D. Collins, C. Luo, G.C. Bazan, T.Q. Nguyen, A.J. Heeger, Adv. Mater. 25 (2013) 1646.
[30] L. Lu, Z. Luo, T. Xu, L. Yu, Nano Lett. 13 (2012) 59.
[31] H. Choi, S.-J. Ko, Y. Choi, P. Joo, T. Kim, B.R. Lee, J.-W. Jung, H.J. Choi, M. Cha, J.-R. Jeong, Nat. Photonics 7 (2013) 732.
[32] G.F. Burkhard, E.T. Hoke, M.D. McGehee, Adv. Mater. 22 (2010) 3293.
[33] J.Y. Kim, S.H. Kim, H.H. Lee, K. Lee, W. Ma, X. Gong, A.J. Heeger, Adv. Mater. 18 (2006) 572.

Gi-Hwan Kim received B.S. degree from Kumoh National Institute of Science of Technology in 2009 and he received Ph.D. from the Department of Chemical and Energy Engineering at Ulsan National Institute of Science and Technology (UNIST) under Professor Jin Young Kim in 2015. He is currently working at the University of Toronto (UT) under Professor Edward H. Sargent (UT) together with Professor Jin Young Kim (UNIST). His current research is focused on the hybrid organic–inorganic optoelectronics and photonics devices by using quantum dot and conjugated polymer.

Dr. Bright Walker received a B.Sc. in Chemistry from UC Berkeley and a Ph.D. in Chemistry from UC Santa Barbara. He is currently a Research Scientist at the Department of Energy Engineering, Ulsan National Institute of Science and Technology. He has currently published 39 papers in peer reviewed journals with 2700 citations and an h-index of 20. His research interests include organic and hybrid semiconducting materials and devices.

Dr. David Zhitomirsky has received his B.Eng. from the McMaster University (Canada) and Ph.D. in photonics from the University of Toronto (Canada). He is currently a postdoctoral associate at the Massachusetts Institute of Technology studying nanoscale energy harvesting in the Grossman group.

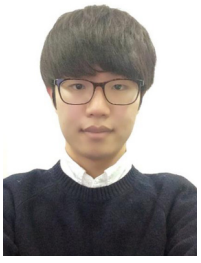

Jungwoo Heo received B.S. degree in both departments of energy conversion & storage, and nanochemistry at Ulsan National Institute of Science and Technology (2012). He is currently a Ph.D. student in Ulsan National Institute of Science and Technology (2012—present). His research interests include colloidal quantum dot materials, devices fabrication, and numerical simulation.

Seo-Jin Ko received B.S. degree from the Chonbuk National University in 2010. He is currently a Ph.D. student in Ulsan National Institute of Science and Technology (2010 —present). His research interests include organic-based solar cells and light emitting diode with various ways to develop the device performance.

Jongnam Park received his B.S. (1999), M.S. (2001), and Ph.D. (2005) from the School of Chemical and Biological Engineering of the Seoul National University, Korea, in the group of Prof. Taeghwan Hyeon. He worked as a postdoctoral associate in the group of Prof. Moungi Bawendi, at the Massachusetts Institute of Technology (MIT), MA, USA. He joined the faculty of the School of Energy and Chemical Engineering at Ulsan National Institute of Science and Technology (UNIST) in 2010, where he has worked and developed the new synthetic methodology of nanomaterials for energy and bio-application.

Ted Sargent holds the Canada Research Chair in Nanotechnology at the University of Toronto, where he also serves as Vice Dean for Research for the Faculty of Applied Science and Engineering. He is a Fellow of the Royal Society of Canada (FRSC), FAAAS, and FIEEE for his contributions to the development of solar cells and light sensors based on solution-processed semiconductors. He is the founder and CTO of InVisage Technologies and of Xagenic Inc.

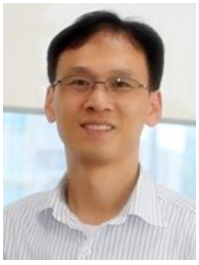

Prof. Jin Young Kim received his B.S. (1998) and Ph.D. in Physics from Pusan National University (2005). He is an Associate Professor in the Department of Energy Engineering, Ulsan National University of Science and Technology (2008.07—present). He served as an Assistant Research Professor in the Heeger Center for Advanced Materials, Gwangju Institute of Science and Technology (GIST) (2007.07–2008) and he was a Post Doc. Researcher in the Center for Polymers and Organic Solids, UC Santa Barbara (Prof. A.J. Heeger) (2005.04–2007.07). His research interests include polymer solar cells, colloidal quantum dot solar cells, and hybrid optoelectronic devices.